Laser Chem. 1988, Vol. 9, pp. 277–288

Reactive Scattering of Oxygen Atoms with Iodine Molecules

N. C. FIRTH, N. W. KEANE, D. J. SMITH and R. GRICE

Chemistry Department, University of Manchester, Manchester M13 9PL

(Received 20 May, 1988)

Reactive scattering of O atoms with I_2 molecules has been studied at an initial translational energy $E \sim 43$ kJ mol^{-1} using cross-correlation time-of-flight analysis with resolutioln improved over previous measurements. The broad centre-of-mass differential cross section favours the backward hemisphere with a product translational energy distribution lying above the distribution observed at lower initial translational energy but below the microcannonical RRHO distribution. However, a minor component with very low product translational energy favours the forward hemisphere. The observed scattering is attributed to a strongly bent OII triplet complex intermediate with a lifetime shorter than the period of overall rotation of the axis of the heavy II diatomic but long compared with the period of vibrational and rotational motion of the light O atom.

KEY WORDS: Molecular beams, reactive scattering, reaction dynamics, oxygen atoms, collision complex.

INTRODUCTION

The reactive scattering of a light atom with a heavy diatomic has recently attracted considerable interest due to the propensity for migratory dynamics[1–4] in such reactions and the possibility of significant correlation effects being observed between the final angular momenta.[5] In the preceding paper[6] a model for the breakdown of long-lived complex dynamics in a light plus heavy–heavy (L + HH) reaction has been applied to O + Br_2 reactive scattering in order to rationalise the increased prominence of the backward scattering observed at high initial translational energy. Previous measurements[7]

on the O + I_2 reaction indicate that similar behaviour is also apparent for this reaction at high initial translational energy. However, a recent RRKM analysis[8] of the laboratory angular distribution of OI scattering suggests that the reaction dynamics may be adequately represented by a long-lived complex model. In order to examine the dynamics of O + I_2 reaction more closely, reactive scattering has been remeasured using a supersonic beam of O atoms seeded in He buffer gas[9] with improved resolution of the OI product velocity distributions.

EXPERIMENTAL

The apparatus and experimental conditions were the same as those used in previous measurements[7] but with the time-of-flight channel width reduced to ~8 μs and a cross-correlation chopper[10] bearing five pseudorandom sequences rotating at 400 Hz. The velocity distribution of the supersonic beam of I_2 molecules seeded in N_2 buffer gas peaked at $v_{pk} \sim 700$ m s^{-1} with a full width at half maximum intensity $v_{wd} \sim 190$ m s^{-1} corresponding to a Mach number M ~ 7.

RESULTS

The laboratory angular distribution of OI number density shown in Figure 1 and the laboratory velocity distributions of OI flux shown in Figure 2 reveal features in the region close to the laboratory centroid which were poorly resolved in the previous measurements. The transformation of these laboratory data to centre-of-mass coordinates employed the stochastic method of Entemann[11] with the differential reaction cross section expressed as a sum of two components each consisting of a product of an angular function $T_i(\theta)$ and a velocity distribution $U_i(u)$

$$I(\theta,u) = T_1(\theta)U_1(u) + T_2(\theta)U_2(u) \quad (1)$$

This two component function proved essential to the analysis of the features now clearly resolved in the experimental velocity distributions. The angular and velocity distributions in Figure 3, show the principal component scattering over the full angular range but favouring the backward hemisphere with a higher product transla-

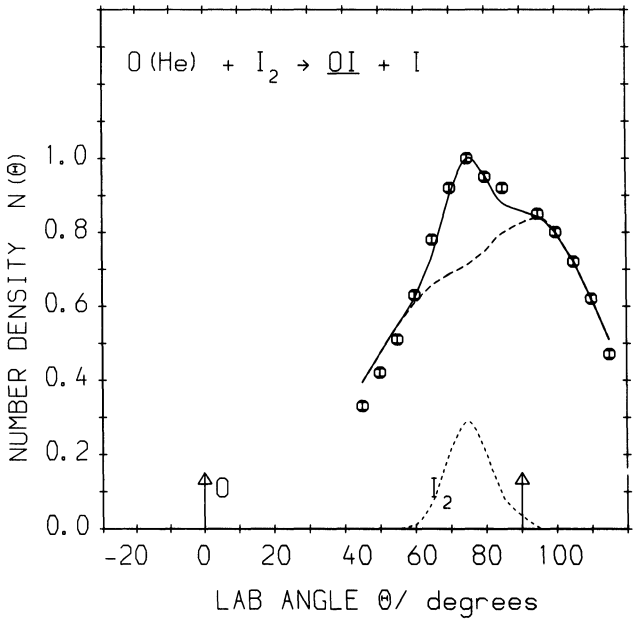

Figure 1 Laboratory angular distribution (number density) of OI reactive scattering at an initial translational energy E = 43 kJ mol^{-1}. The overall fit of the Entemann kinematic analysis shown by solid curve, the contributions of the separate components by broken curves.

tional energy than the minor component which favours the forward hemisphere with a very low product translational energy. The fits of the stochastic analysis are shown by a solid curve in Figure 1 and broken curves in Figure 2. The contributions of the separate components to the laboratory angular distribution are shown by broken curves in Figure 1. While the principal component makes the major contribution to the OI number density over the full angular range, the minor component makes an important contribution in the angular range close to the laboratory centroid. This accords with the features observed in the laboratory velocity distributions lying close to the laboratory centroid. The peak E'_{pk} and average E'_{av} product translational energies are listed in the table for each component together with the initial translational energy E and the reaction exoergicity ΔD_0. The composite angular function $T(\theta) = T_1(\theta) + T_2(\theta)$ and the product

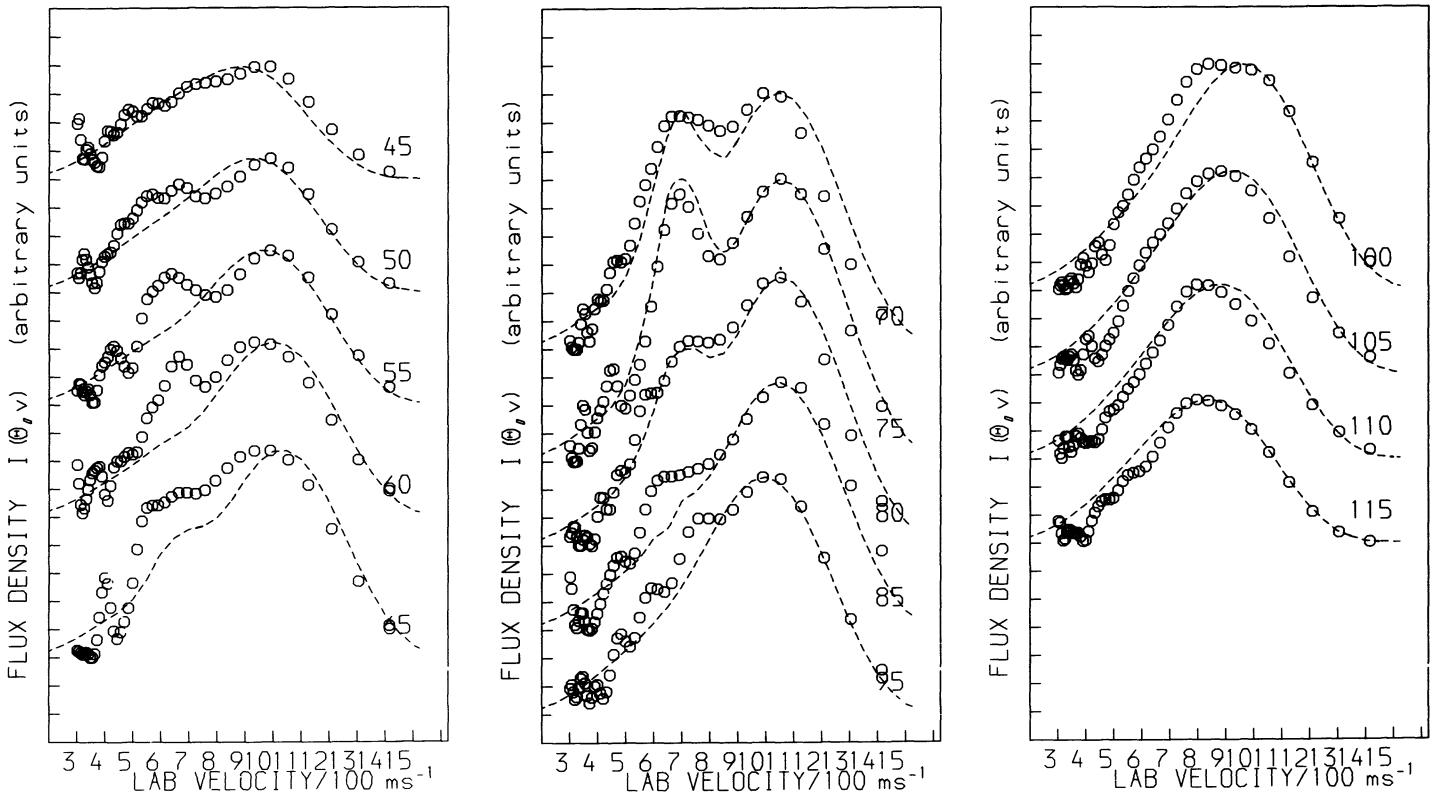

Figure 2 Laboratory velocity distribution (flux density) of reactively scattered OI from O + I_2 at an initial translational energy $E = 43$ kJ mol^{-1}. The overall fit of the Entemann kinematic analysis is shown by broken curves.

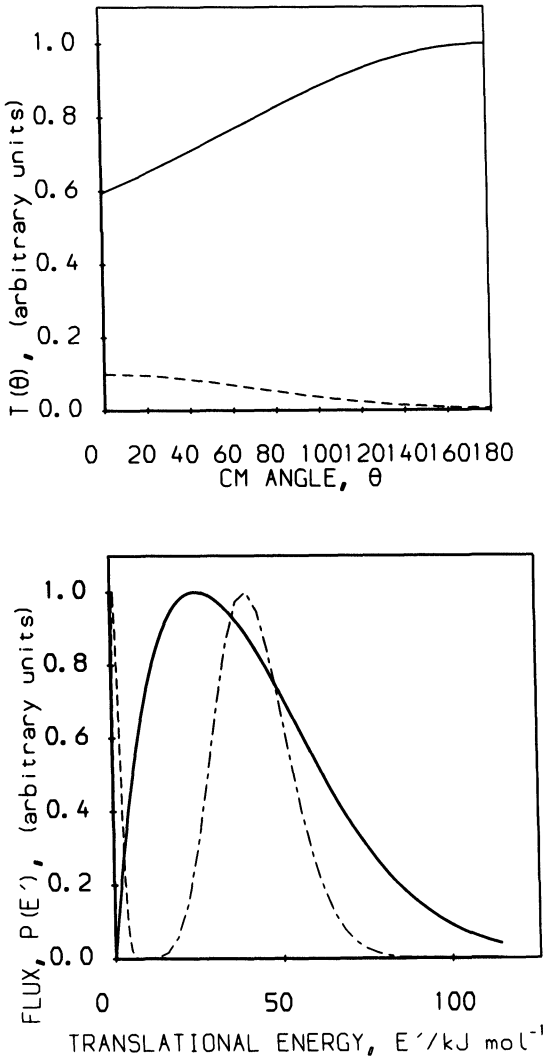

Figure 3 Component angular functions $\mathbf{T}(\theta)$ and translational energy distributions $P(E')$ for O + I_2 at an initial translational energy E = 43 kJ mol^{-1}. Major component is shown by a solid curve, minor component by a broken curve and the distribution of initial translational energy by a dot–dash curve.

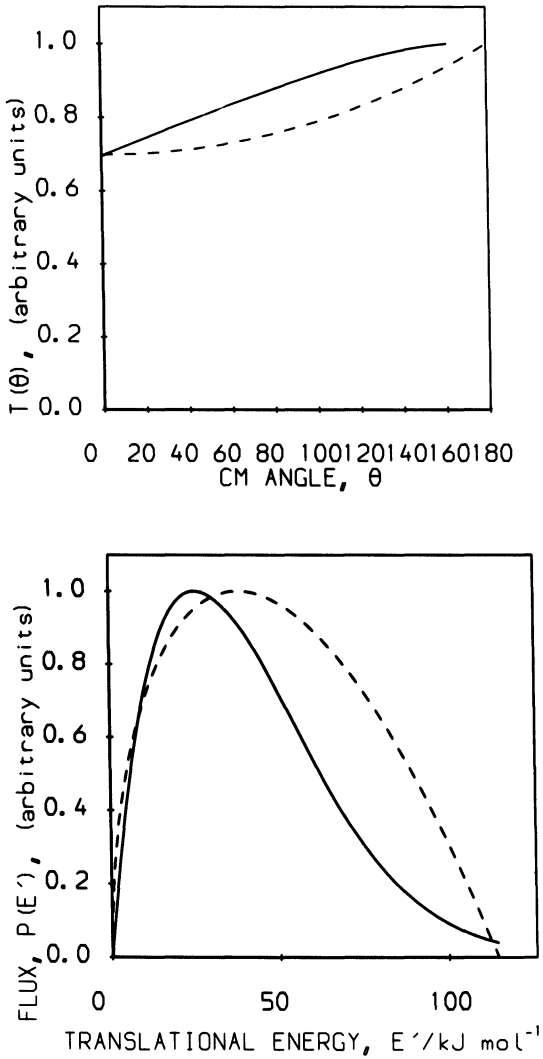

Figure 4 Composite angular distribution and translational energy distribution for backward scattering shown by solid curves. Angular distribution of Eq. (4) for short-lived complex and microcannonical RRHO prediction of Eq. (5) for the product translational energy distribution are shown by broken curves.

translational energy distribution for backward scattering are shown in Figure 4. The composite angular function is similar to that for the principal component but with slightly increased scattering in the forward direction. The composite product translational energy distribution for forward scattering differs from that of the backward scattering only at very low translational energy. Indeed the contribution of the minor component to the total reaction cross section may be determined by integration over the centre-of-mass angular and velocity distributions

$$Q = \int_0^{\pi} T(\theta) \sin \theta d\theta \int_0^{u_{max}} U(u) du \tag{2}$$

This gives an estimate of only ~0.2% for the minor component, and its prominence in the laboratory scattering may be attributed to the kinematic enhancement[11] of OI product with very low centre-of-mass velocity.

DISCUSSION

The geometry of the OII triplet complex is predicted by Walsh molecular orbital theory[12] to be more strongly bent than the OBrBr complex due to the lower electronegativity of the central I atom compared with the Br atom. As in the interbond angle β decreases, the model presented in the preceding paper[6] for the angular distribution of reactive scattering generated by precession of a bent long-lived complex[13]

$$T(\theta) = (2/\pi) \arcsin (\sin \gamma / \sin \theta) \quad \text{for} \quad \sin \theta > \sin \gamma$$
$$T(\theta) = 1 \quad \text{for} \quad \sin \theta \leqslant \sin \gamma \tag{3}$$

has progressively broader forward and backward peaking. However, the limit of an isotropic angular distribution with $\gamma = 90°$ is reached only when the preferred geometry of the complex has a symmetrical isosceles triangular configuration IOI. The composite angular function $T(\theta)$ of Figure 4 shows OI scattering over the full angular range favouring the backward direction. If it is assumed that precessing complexes have an exponential distribution of lifetimes according to the osculating complex model,[14–17] the density of complexes declines over successive half periods of rotation. If it is also assumed that precession commences with a scattering angle $\theta = \pi$ for complexes

formed in small impact parameter collisions and that the angular distribution for a very long complex lifetime approximates to isotropic, then the angular distribution generated for a finite lifetime may be written

$$T(\theta) = e^{-(\pi-\theta)/\theta^*} + e^{-(\pi+\theta)/\theta^*} + e^{-(3\pi-\theta)/\theta^*} + e^{-(3\pi+\theta)/\theta^*} + \ldots$$
$$= 2\cosh(\theta/\theta^*)\{e^{-\pi/\theta^*} + e^{-3\pi/\theta^*} + \ldots\}$$

Normalising to unity at $\theta = \pi$ yields

$$T(\theta) = \cosh(\theta/\theta^*)/\cosh(\pi/\theta^*) \quad (4)$$

where $\theta^* = 2\pi\tau/T$ and τ denotes the complex lifetime and T the rotational period. The angular distribution corresponding to Eq. (4) with $\theta^* = 200°$, shown by a broken curve in Figure 4 agrees quite well with the composite angular distribution shown by a solid curve, although the shape of the broken curve is concave upward compared with the convex shape of the experimental curve. This discrepancy in shape may well arise from the approximations invoked in deriving the simple limiting form of Eq. (4). In particular the discussion of backward scattering for O + Br_2 in the preceding paper[6] indicates that the distribution of initial angles for complex precession in small impact parameter collisions may be closer to a cosine distribution than the single value $\theta = \pi$ used in deriving Eq. (4). The nominal lifetime $\tau \sim 0.56\ T$ corresponding to the parameter $\theta^* = 200°$ indicates that OII complexes precess for roughly one half period of overall rotation of the principal axis of the complex which approximates to the axis of the heavy I–I diatomic. In the case of the O + Br_2 reaction[6] the product translational energy distribution for scattering in the backward direction was found to be well represented by the microcannonical RRHO prior distribution[18]

$$P(f') = (3^{3/2}/2)f'^{1/2}(1 - f') \quad (5)$$

where $F' = E'/(E + \Delta D_0)$. The RRHO distribution shown by a broken curve in Figure 4, predicts rather higher product translational energy than that exhibited by the experimental distribution shown by a solid curve.

The rate constant $k = 8.4 \times 10^{10}$ dm^3 mol^{-1} s^{-1} for the O + I_2 reaction measured[19] at 298 K corresponds to a total reaction cross section $Q \sim 25$ Å^2 which is considerably greater than that $Q \sim 2.5$ Å^2 for O + Br_2. Indeed RRKM calculations[20] indicate that there is no

energy barrier in the entrance valley of the potential energy surface for O + I_2 but that reaction is still confined[8] to quite small impact parameters $b \lesssim 3$ Å. If bond lengths of $r(OI) \simeq 2.0$ Å and $r(I_2) \simeq 2.8$ Å are adopted for an OII triplet complex with an interbond angle $\beta \sim 120°$, as has recently been proposed for the preferred geometry of the FII transition state in the F + I_2 reaction,[1] then a collision radius $R \sim 3$Å is predicted by the collision complex model in the preceding paper.[6] This preferred geometry for the OII triplet complex yields $\gamma \sim 36°$ which gives an angular function $T(\theta)$ according to Eq. (3) with quite pronounced forward and backward peaking. Such an angular distribution is in accord with the experimental distributions determined[7,21] at lower initial translational energy but not with the more nearly isotropic distribution determined in the present experiments at higher initial translational energy. Similarly the product translational energy distribution determined[7,21] at low initial translational energy peaks at a low product translational energy corresponding to the maximum centrifugal barrier[22]

$$B'_m = (\mu/\mu')E \tag{6}$$

where μ, μ' denote the initial and final reduced masses. At the higher initial translational energy of the present experiments the product translational energy distribution for the major component peaks well above the centrifugal barrier $B'_m \sim 10$ kJ mol^{-1} predicted by Eq. (6), but the minor component peaks at much lower energy.

The experimental data for O + I_2 at high initial translational energy follow the short-lived complex model proposed in the preceding paper[6] where the complex lifetime is shorter than the period of overall rotation of the symmetry axis of the OII triplet complex which is approximately the I—I bond axis, but the lifetime is long compared with the period of O atom vibrational and rotational motion. However, the OII complex is more strongly bent than the OBrBr complex and the OI reactive scattering depends both on impact parameter and on the initial angle of inclination between the I_2 molecule axis and the plane of collision. Consequently the angular distribution of reactive scattering is not so directly related to impact parameter as is the case for the O + Br_2 scattering. Thus the product translational energy distribution for the principal component of the O + I_2 scattering does not vary with scattering angle and peaks at an energy intermediate between the maximum centrifugal barrier and the prediction of the

microcannonical RRHO distribution. The minor component of the O + I_2 reactive scattering, which favours the forward hemisphere and has a very low product translational energy, may be related to the limiting configuration of large impact parameter collisions with the I_2 molecule axis initially strongly inclined to the plane of collision as illustrated in Figure 5. In this configuration the component of the initial orbital angular momentum perpendicular to the I—I bond axis $L \sin \gamma$ gives a centrifugal barrier[23]

$$B' = B'_m \sin^2\gamma \tag{7}$$

which is much lower $B' \sim 3.5$ kJ mol^{-1} than the maximum centrifugal barrier B'_m given by Eq. (6) for the in plane scattering and is comparable to the product translational energy for the minor component of the OI reactive scattering given in the table.

The reaction dynamics for O + Br_2 and O + I_2 have been discussed in terms of motion over the triplet potential energy surface[24] but these surfaces are underlain by a singlet surface with a deep minimum corresponding to the symmetrical isosceles triangular configuration.[25] Thus singlet character induced by strong spin–orbit interaction may contribute to the wavefunction of the potential energy surface for strongly bent configuration of the triplet complex shown in Figure 5.

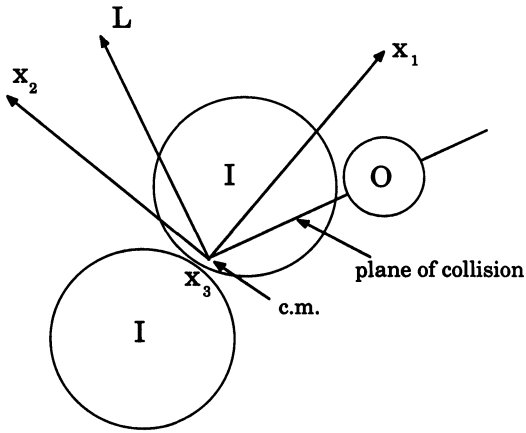

Figure 5 Proposed triplet complex for the O + I_2 reaction. Principal axes of the complex are denoted, x_1, x_2 with x_3 perpendicular to the plane of the complex. The initial orbital angular momentum **L** is perpendicular to the plane of collision.

Table I Reaction energetics; initial translational energy E, peak E'_{pk} and average E'_{av} product translational energies and reaction exoergicity ΔD_0.

Component	E/kJ mol^{-1}	E'_{pk}/kJ mol^{-1}	E'_{av}/kJ mol^{-1}	ΔD_0/kJ mol^{-1}
Major	43	26	41	73 ± 5
Minor		1	2	

The reactive scattering[5] arising from such a symmetrically bound singlet intermediate would necessarily exhibit symmetry about $\theta = 90°$ and because of the long-range attractive interaction induced by the oxygen atom lying between the halogen atoms on the singlet surface, would give rise to in plane scattering with low product translational energy. However, there is little evidence for sharply forward–backward peaked scattering in the O + I_2 reaction and for the O + Br_2 reaction the observed sharp forward peaking may be attributed to a triplet intermediate which is not strongly bent.[6] Hence the dynamics of the O + Br_2 and O + I_2 reactions appear to be confined mainly to the triplet potential energy surface, which must therefore be separated from the singlet surface by an energy barrier in strongly bent configurations.

Acknowledgement

Support of this work by SERC is gratefully acknowledged.

References

1. N. C. Firth, N. W. Keane, D. J. Smith and R. Grice, *Faraday Discuss.* **84**, 53 (1988).
2. I. W. Fletcher and J. C. Whitehead, *Faraday Trans. II* **78**, 1165 (1982).
3. I. W. Fletcher and J. C. Whitehead, *Faraday Trans. II* **80**, 985 (1984).
4. M. I. Urrecha, F. Castano and J. Iturbe, *Faraday Trans. II* **82**, 1077 (1986).
5. S. K. Kim and D. R. Herschbach, *Faraday Discuss.* **84**, 159 (1988).
6. N. C. Firth, N. W. Keane, D. J. Smith and R. Grice, *Laser Chem.* **9**, 265 (1988).
7. A. Durkin, D. J. Smith and R. Grice, *Molec. Phys.* **46**, 1251 (1982); **48**, 1137 (1983).
8. P. A. Elofson, K. Rynefors and L. Holmlid, *Chem. Phys.* **118**, 1 (1987).
9. P. A. Gorry and R. Grice, *J. Phys. E* **12**, 857 (1979).
10. C. V. Nowikow and R. Grice, *J. Phys. E* **12**, 515 (1979).
11. E. A. Entemann and D. R. Herschbach, *Faraday Discuss.* **44**, 289 (1967).
12. A. D. Walsh, *J. Chem. Soc.* 2266 (1953); D. R. Herschbach, Proc. Conf. on Potential Energy Surfaces in Chem. (W. A. Lester, Ed.), 44 (1970).
13. N. W. Keane and R. Grice, *Molec. Phys.* **61**, 869 (1987).

14. G. A. Fisk, J. A. McDonald and D. R. Herschbach, *Discuss. Faraday Soc.* **44**, 228 (1967).
15. M. K. Bullitt, C. H. Fisher and J. L. Kinsey, *J. Chem. Phys.* **60**, 478 (1974).
16. S. Stolte, A. E. Procter and R. B. Bernstein, *J. Chem. Phys.* **65**, 4990 (1976).
17. W. R. Creasy and J. M. Farrar, *Faraday Discuss.* **84**, 281 (1988).
18. R. D. Levine and R. B. Bernstein, Molecular Reaction Dynamics and Chemical Reactivity (Oxford University Press, 1987).
19. G. W. Ray and R. T. Watson, *J. Phys. Chem.* **85**, 2955 (1981).
20. K. Rynefors, L. Holmlid and P. A. Elofson, *Chem. Phys.* **118**, 417 (1987).
21. D. D. Parrish and D. R. Herschbach, *J. Amer. Chem. Soc.* **95**, 6133 (1973); D. St. A. G. Radlein, J. C. Whitehead and R. Grice, *Molec. Phys.* **29**, 1813 (1975).
22. S. A. Safron, N. D. Weinstein, D. R. Herschbach and J. C. Tully, *Chem. Phys. Lett.* **12**, 564 (1972).
23. S. M. A. Hoffmann, D. J. Smith, A. Gonzalez Urena, T. A. Steele and R. Grice, *Molec. Phys.* **53**, 1067 (1984).
24. R. Grice, *Chem. Soc. Rev.* **11**, 1 (1982).
25. C. Campbell, J. P. M. Jones and J. J. Turner, *Chem. Commun.* 888 (1968).